Heliyon 10 (2024) e29337

Contents lists available at ScienceDirect

Heliyon

journal homepage: www.cell.com/heliyon

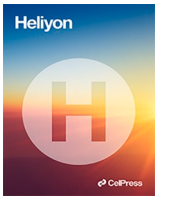

Research article

Surface topography, structural, optical and dc electrical behaviors of pristine and Co-doped ZnS thin films

Rahima Nasrin [a,*], Lamiya Khan [a], Md Obaydul Haq [a], Md Mohiuddin [a], Humayun Kabir [b]

[a] Department of Physics, University of Barisal, Barisal, 8200, Bangladesh
[b] Department of Physics, Jahangirnagar University, Savar, Dhaka, 1342, Bangladesh

ARTICLE INFO

Keywords:
Chemical bath deposition
Doping
Optical behavior
Thin films
Zinc sulfide
XRD properties

ABSTRACT

The prime goal of the present research is to synthesize pristine zinc sulfide (PZS) and cobalt (Co)-doped zinc sulfide (CDZS) thin films with different doping concentrations (DC) via chemical bath deposition (CBD) method. The effect of Co-doping on the surface topography, structural, optical and dc-electrical behaviors of PZS thin films has been ascertained. Scanning electron microscopy images exhibited nearly sphere-shaped agglomerates of grains dispersed throughout the surface with cracks in PZS thin film whereas cracks were absent in CDZS. Atomic force microscopy image displayed smooth surface of CDZS thin film with evenly dispersed small grains. The hexagonal wurtzite structure of PZS and CDZS thin films with varied X-ray diffraction (XRD) parameters was confirmed via XRD analysis. Optical investigation revealed that the optical direct band gap energy increased with decreasing DC from 12 % to 4 %. Alteration of other optical parameters namely absorption coefficient, extinction coefficient, refractive index, real and imaginary parts of dielectric constant, etc. with DC was also discussed. Direct current electrical investigation revealed that the current-voltage characteristics are linear for all thin films signifying that the electrical conduction in CDZS is ohmic in nature.

1. Introduction

Now-a-days thin film (TF) technology is advancing remarkably to develop novel materials namely nanomaterials, biomaterials, magnetic materials, graphene, metal-organic framework, etc. [1,2]. Zinc sulfide (ZnS) is a compound semiconductor of II-VI group which has drawn the attention of many researchers due to its excellent properties and numerous potential optoelectronic and spintronic applications for example flat panel displays [3], injection lasers [4], light emitting diodes [5], cathode ray tubes [6], thin film luminescence [7], buffer layer in the solar cell [8], etc. Nevertheless, to exploit some additional properties as well as enhance its physico-chemical properties, pure ZnS (PZS) thin film has been tailored by doping it with transition metals like Fe [9], Ni [10], Mn [11], Cu [12] and Co [13]. PZS doped by these transition metals has received much attention because this permits researchers to enhance many functions by transporting and controlling various types of spin. The metal doping concentration (DC) may alter the energy band gap (E_g) and affect photoluminescence (PL) due to the creation of different trap centers as compared to the PZS [14–17]. Among several transition metal doping elements, the high solubility of Co, (30 %) makes the doping process with ZnS possible, faster and easy. Much research displayed that Co seems to be a highly favored doping element that can enhance the optical and PL properties

* Corresponding author.
E-mail addresses: muktanasrin77@gmail.com, drnasrin@bu.ac.bd (R. Nasrin).

https://doi.org/10.1016/j.heliyon.2024.e29337
Received 23 December 2023; Received in revised form 4 April 2024; Accepted 5 April 2024
Available online 11 April 2024

of II-VI semiconductor thin film [15,18]. Generally, Co-doped ZnS (CDZS) provides new opportunities for full-color luminescence in the UV–visible region which is used for various applications as well as research purposes. CDZS displayed stronger coupling owing to the mixing of Co d-orbital with the valence band and conduction band of the II-VI materials [19]. Semiconductor thin films (STF) can be deposited via diverse methods namely chemical vapor deposition (CVD) [20], chemical bath deposition (CBD) [21–23], plasma-assisted CVD [24], SILAR method [25], pulsed laser deposition [26], electrodeposition [27], spray pyrolysis [28], and atomic layer epitaxy [29], etc. Among these, the CBD method nabbed attention as it is a budget-friendly, simple and low-temperature technique for producing STF [30]. Substantial research works have been performed on STF synthesized by CBD techniques. Aksay et al. [31] reported the structural and optical behaviors of Sn-doped ZnO thin films synthesized by the CBD method. X-ray diffraction patterns indicated the hexagonal structure of these STFs. With the increase of Sn dopant, the intensity of transmittance (*T*%) spectra is increased within the range 200–900 nm and the E_g is increased from 3.27 to 3.37 eV. The surface roughness declined with the increasing DC as detected by atomic force microscopy. Goudarzi et al. [11] prepared CBD-deposited Mn-doped ZnS thin films. The consistent and dense narrow film surface was observed by field emission scanning electron microscopy (FESEM). The optical study revealed that the films were exceedingly transparent (>80 %) in the visible region. Ashok et al. [32] prepared cadmium sulfide thin films (CSTF) via CBD technique and different characterizations were done. The CSTF grows in a stable hexagonal wurtzite structure having a favored orientation along the (002) lattice plane. Even, grainy, and plane surfaces with an average grain size of less than 100 nm were observed by FESEM. The E_g were obtained in the range of 2.3–2.35 eV of CSTF. Maria et al. [33] prepared PZS and Al-doped ZnS thin films by CBD method onto glass substrates at 85 °C. XRD pattern exhibited a hexagonal wurtzite crystal structure and showed (008) preferential orientation. The FESEM images exhibited that the glass substrate was nicely covered by compact and dense mosaic-like nanostructures. UV–visible analysis exposed that approximately 70%–80 % *T*% happened in the visible to near-infrared region, with an E_g in the range of 3.52 eV–3.76 eV.

The literature review is evident that there are scanty reports on the investigation of CDZS thin films. Particularly, it is the least studied material regarding different optical parameters and electrical properties. In this research, PZS and CDZS thin films were deposited onto a glass substrate via CBD method. To understand the effect of Co-doping on the various properties of PZS and to correlate these, the topographical, compositional, structural, photosensitive and dc-electrical behaviors of the deposited thin films (TF) were investigated using SEM, AFM, energy dispersive X-ray spectroscopy (EDX), XRD, UV–vis spectroscopy and four-point probes method, respectively. It is projected that these analyses may put light on its improved properties after Co-doping that may be suitable for some device applications.

2. Experimental details

2.1. Materials and method

All the reagents used for the synthesis of TF were analytical grade. 0.2 M Zinc acetate (40 ml), 0.4 M thiourea (80 ml), 0.2 M tri-sodium citrate dehydrate (60 ml), 25 % ammonia solution (20 ml) and cobalt chloride hexahydrate were used for the solution. In the present work, glass slides were utilized as substrate. The substrates were cleaned with liquid detergent, ethanol, HCl solution separately for 30 min followed by rinsing in distilled water. After cleaning with acid, the glass substrates were ultrasonically cleaned with acetone and de-ionized water each for 10 min. Finally, glass substrates were dried naturally in the air. First, 0.4 M thiourea and 0.2 M zinc acetate were mixed separately with de-ionized water and stirred for 15 min to make a homogenous solution using a magnetic stirrer. Then, 0.2 M tri-sodium citrate was added to the zinc acetate solution and stirred for 10 min. Thereafter, the earlier prepared thiourea solution was mixed with it under a rousing condition to get a clear and homogenous solution followed by an accumulation of cobalt chloride hexahydrate in proper amount to attain the chosen doping levels from 4 to 16 wt%. Lastly, a proper amount of de-ionized water was assorted to make it a 200 ml solution and 25 % ammonia solution was also mixed with it by a CBD system to make the solution alkaline. The beaker of the homogenous solution was placed in the heat chamber of CBD system under a stirring condition. The pH was maintained at 10 which was confirmed using a pH indicator strip. The solution was heated to 80 °C. Then, one pre-cleaned glass substrate was placed vertically inside the bath. After deposition of 2 h, the sample was collected and washed through de-ionized water. The thin film samples were dried naturally and well-kept up in a sealed container. The thickness of the TF was measured by using the multiple-beam interferometry technique [34]. By using this technique, the thickness, *d* of the prepared thin films was computed using the following equation (1) [34]:

$$d = \lambda q/2p \tag{1}$$

where, *p*, *q,* and λ are the fringe width, step height of the fringe, and wavelength of the used sodium light, respectively. The estimated thicknesses are 183, 150, 135 and 125 nm for PZS, 4 %, 8 % and 12 % CDZS thin films, respectively. The possible reactions for the formation of ZnS can be presented by the following equations [35]:

$$Zn\ (CH_3COO)_2 \rightarrow 2CH_3COO^- + Zn^{2+}$$

$$NH_4OH \rightarrow NH_4^+ + OH^-$$

$$SC(NH_2)_2 + OH^- \rightarrow CH_2N_2 + SH^- + H_2O$$

$$SH^- + OH^- \rightarrow S^{2-} + H_2O$$

$$Zn[Na_3C_6H_5O_7] + SC(NH_2)_2 + 2OH^- \rightarrow ZnS + Na_3C_6H_5O_7 + CO(NH_2)_2 + H_2O$$

For Co doped ZnS thin films, the possible chemical reactions are

$$CoCl_2 \rightarrow Co^{2+} + 2Cl^-$$

$$Co^{2+} + OH^- \rightarrow Co(OH)_2^-$$

$$Co(OH)_2 + OH^- \rightarrow Co(OH)_3^-$$

$$ZnS + Co(OH)_3^- \rightarrow ZnS{:}Co$$

2.2. Characterization techniques of thin films

The PZS and CDZS thin film surfaces were analyzed through a scanning electron microscope (SEM) (EVO18, Carl Zeiss AG, UK). The functional voltage and magnification of the SEM were 30 kV and × 25 k, respectively. The analysis of compositional elements of the prepared samples was completed through an EDX spectrometer (EDAX Team, EDAX, USA). AFM analysis was carried out through an AFM (Nanosurf, model- FLEXAFM, Switzerland). The structural characterization was performed by BRUKER D8 X-ray diffractometer (Netherlands) using Cu-K_α radiation of wavelength 1.5418 Å across a 2θ range of 15-60°. A dual-beam UV–Vis spectrophotometer (Shimadzu UV-1601, Japan) was used for optical analysis of the prepared samples in the spectral range 300–1100 nm. Finally, absorbance data were used to estimate optical parameters. Dc electrical investigation was done by a four-point probe system (Ossila, UK).

3. Results and discussion

3.1. SEM analysis

Fig. 1 (a, b) displayed SEM images of (a) PZS and (b) a representative 8 % CDZS thin films at ×25 K magnifications respectively. The SEM images displayed different surface morphologies as the presence of doping element with PZS. The PZS thin film has a non-uniform surface with a crack and sphere-shaped agglomerates of grains are dispersed through the substrate surface. The size of grain is tiny and their distribution is more even without any crack in CDZS in comparison to PZS one, which is suitable for optoelectronic applications. The agglomerates' number appears to decrease in the existence of cobalt content. Previously Akhtar et al. [36] observed that the absence of crack and almost equal size spherical clusters are present in their CDZS thin films.

3.2. EDX analysis

The EDX spectra of a representative 8 % CDZS thin film and in the inset table for weight % and atomic % of different elements present in this film are exhibited in Fig. 2. The sturdy and sharp peaks of Zn and S elements and weak peak for Co content are observed in EDX spectra. In the spectrum there were no additional elements were observed, which confirms the purity of the samples.

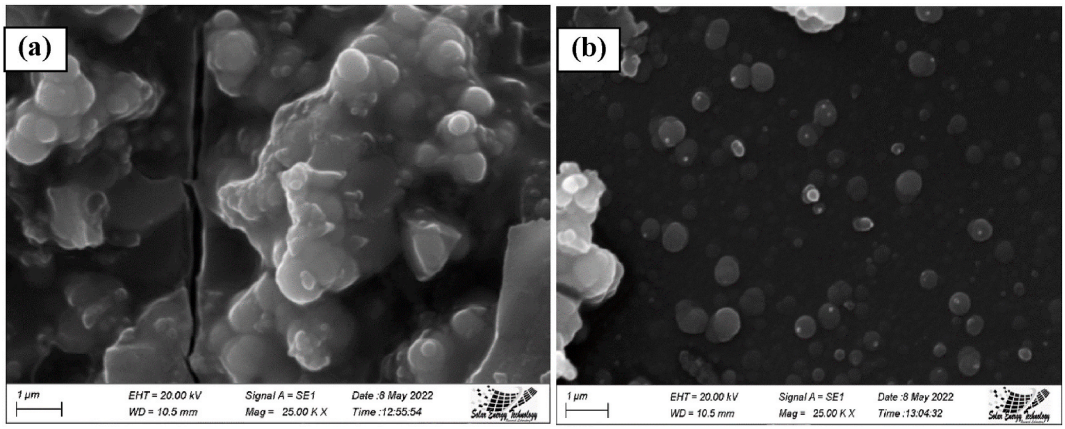

Fig. 1. SEM image of (a) PZS and (b) 8 % CDZS thin film at × 25K magnification.

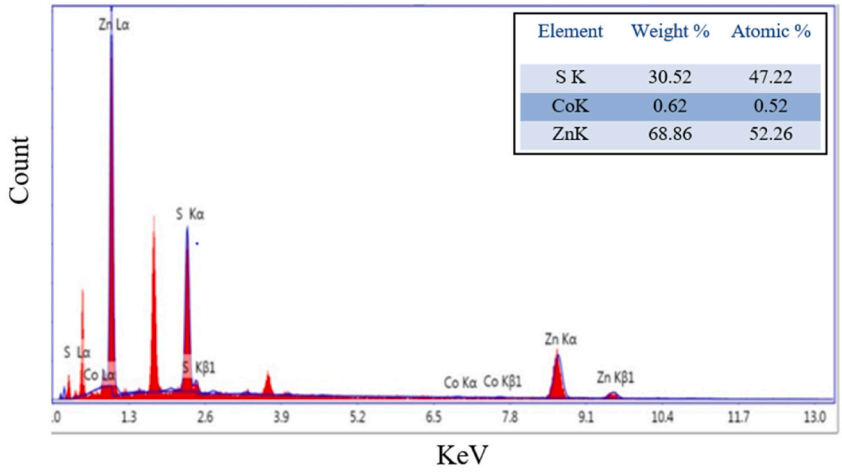

Fig. 2. EDX spectra of a representative 8 % CDZS thin film (inset table for weight % and atomic % of different elements present in 8 % CDZS thin films).

3.3. AFM analysis

The 2-D topographical image of a representative 8 % CDZS thin film is demonstrated in Fig. 3. The film displayed a smooth surface with fairly distributed small spherical shaped grains over an area of 10.6 × 10.6 μm^2 with root-mean-square (RMS) roughness of 28 nm.

3.4. XRD analysis

Fig. 4 exhibited the XRD pattern of PZS and CDZS thin films deposited under different DC. It is observed that a diffraction peak at 2θ values of 20.62°, 20.36°, 20.64° and 20.54° respectively for PZS, 4 %, 8 %, and 12 % due to reflection from the (102) plane. The XRD pattern also corresponds to diffraction patterns of the hexagonal structural phase which agreed with the reported JCPDS data card no: 01-074-5003 [37]. The peak (102) originated at around $2\theta = \sim 21^\circ$ in the PZS and CDZS is basically due to the ZnS phase. However, there might be an impurity phase like $Zn(OH)_2$ [38] which merged with the PZS and CDZS phase. With the increase of doping content, the intensity of this peak (at 21°) decreased. Finally at 12 % CDZS thin films two new peaks at 2θ values of 23° and 32° have been observed, which indicated the hexagonal structures of the films. A similar type of structural orientation was observed by Khalil et al. et al. [39] for deposition parameter-dependent ZnS thin films prepared by the CBD method where a broad peak has been formed at around $2\theta = \sim 22^\circ$and a sharp peak at around $2\theta = \sim 32^\circ$ (104 plane) which signifying hexagonal structures of the films. From Fig. 4, it was also identified that the intensity of sharp and strong peak present at (102) crystal plane of PZS thin film decreased with increasing DC but an increase in DC caused the emergence of crystal planes [(110) and (104)] in the CDZS thin films (12 % CDZS). In contrast, Heiba et al. [13] prepared CDZS thin films using thermolysis method and in XRD pattern they observed a single-phase cubic zinc blende

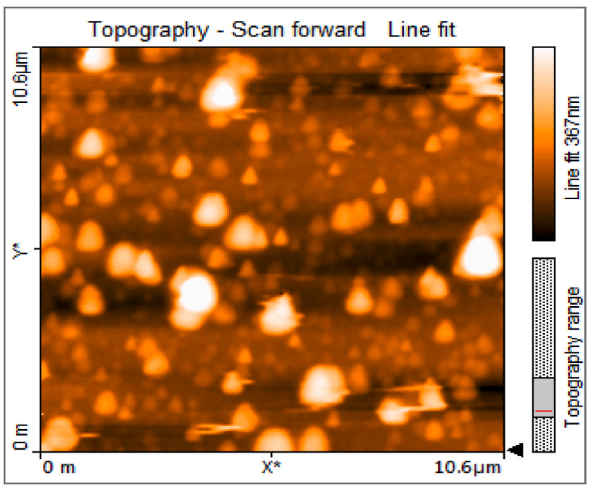

Fig. 3. AFM image of a representative 8 % CDZS thin film.

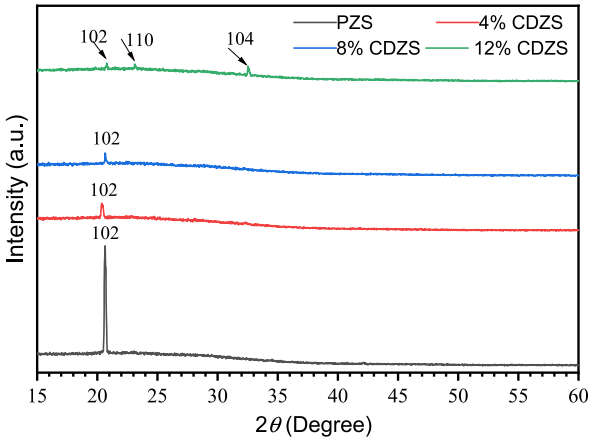

Fig. 4. XRD pattern of PZS and CDZS thin films at variable doping concentration.

structure. In another study [40], the observed CBD-deposited.

PZS thin film was amorphous in nature and annealed zinc sulfide (AZS) thin film became polycrystalline in nature with only one weak diffraction peak corresponding to the (008) plane of the hexagonal ZnS. This discrepancy may be attributed to the different deposition processes and parameters. Structural parameters namely crystallite size (D), dislocation density (δ), micro-strain (ε), number of crystallites per unit area (N) and interplanar spacing (d) were computed by the subsequent equations (2)–(6), respectively [[41–43,43,44]:

$$D = \frac{0.9\lambda}{\beta \cos\theta} \tag{2}$$

$$\delta = \frac{1}{D^2} \tag{3}$$

$$\epsilon = \frac{\beta \cos\theta}{4} \tag{4}$$

$$N = \frac{t}{D^3} \tag{5}$$

$$\frac{1}{d^2} = \frac{4}{3}\frac{h^2 + k^2 + l^2}{a^2} + \frac{l^2}{c^2} \tag{6}$$

Where β is the full width at half maximum of the diffraction angles, λ is the wavelength of Cu-Kα radiation, a is the lattice constant and θ is the diffraction angle. All the calculated XRD parameters of PZS and CDZS thin films are compiled in Table 1. Table 1 displayed that with increasing DC, the lattice parameter, a of the thin films decreased. The lattice parameter (a) decreases due to the smaller ionic radius of Co^{2+} (0.072 nm) as compared to Zn^{2+} ions(0.074 nm) indicating that the CDZS lattice is under compressive strain due to smaller radii of Co^{2+} ions [45]. The calculated average crystallite size of the PZS thin film was 30.9 nm which is larger than CDZS thin films. For 4 %, 8 %, and 12 % Co, the average crystallite size was 23.9, 26.0, and 28.2 nm, respectively. ZnS thin film doped with 4 % cobalt revealed the lowest average crystallite size. Thus, it can be said that the particle size is reduced due to co-doping.

The decrease in crystallite size with doping was also observed by Mukherjee et al. [46] in tin-doped ZnS thin films prepared using CBD process. From Tables 1 and it is also noticed that the microstrain in the ZnS thin films increased due to Co-incorporation. The value of microstrain enhanced from 1.12×10^{-3} for PZS to 1.45×10^{-3} for 4 % CDZS film. The decrease in average particle size might be due to the enhancement of strain in the film. Similar effects of decrease of particle size with increasing strain have been reported for Cd-doping in ZnO thin film [47].

Table 1
Structural parameter of PZS and CDZS thin films.

Samples type	Experimental		Standard (JCPDS no. 01-074-5003)		β	A	c	D	$\delta \times 10^{-3}$	$\varepsilon \times 10^{-3}$	$N \times 10^{-3}$
	2θ (°)	d	2θ (°)	d	(rad)		(nm)	(nm^{-2})	(nm^{-2})		
PZS	20.61	4.35	20.12	4.41	0.0046	3.83	8.66	30.9	1.04	1.12	6.18
4 % CDZS	20.36	4.30	–	–	0.0059	3.81	8.77	23.9	1.74	1.45	10.9
8 % CDZS	20.64	4.32	–	–	0.0054	3.80	8.65	26.0	1.48	1.33	7.71
12 % CDZS	20.78	3.94	–	–	0.0050	3.79	8.59	28.2	1.26	1.23	5.61

3.5. Optical properties

3.5.1. Absorbance

Fig. 5 displayed the absorbance (A) Vs wavelength (λ) curve for PZS and CDZS thin films with different doping concentrations. The absorbance spectra are dropped rapidly with the λ.

within the UV region (UVR) then decreases slowly in the visible region (VR) and later it becomes nearly flat in the IR region. All TF demonstrated higher A value in the UVR making it helpful as a windscreen covering and driving mirror to predict the effect of striking light into a driver's eyes from a forthcoming vehicle and next vehicle [31]. The maximum A is observed for PZS thin film. With increasing Co-doping concentration, the A value of the TFs decreased within the considered range of λ.

3.5.2. Transmittance

The variation of transmittance, T (%) spectra with wavelength of PZS and CDZS thin films at diverse DC is demonstrated in Fig. 6. It can be noticed that with the rise of Co-doping concentration, the $T\%$ of the TF's surges and all TFs have higher $T\%$ values in the visible range indicating the result of the wide E_g of the TF. The maximum $T\%$ is about 50 % for 12 % CDZS thin film at 750 nm. From the previously reported work [19] it is displayed that with the increase of wavelength, the $T\%$ increases for CDZS thin films and the maximum $T\%$ was found to be 45 % in VR which is in good agreement with our works. However, another study revealed that [36,45] the maximum $T\%$ of CDZS thin films is about 80 % at VR. This might have happened due to variation of reagent in preparation of precursor solution or the slower reaction rate. Another observation is that in our case the presence of cracks and sphere-shaped agglomerates of grains were detected by SEM analysis whereas a smooth surface of no crack and almost equal size spherical clusters are present in their [36] CDZS thin films.

3.5.3. Refractive index

The refractive index (n) was computed using the following equation (7) [48]:

$$n = \frac{1+\sqrt{R}}{1-\sqrt{R}} \tag{7}$$

The n vs λ curve for PZS and CDZS thin films at diverse DC is illustrated in Fig. 7. It is detected that the value of n decreased with the rising of Co concentration. This might have happened due to the increase in the number of voids. Göde et al. [49] reported the reverse nature in their work where the n values of PZS increase with increasing Cu and Mn concentrations. It is also worth noting from Fig. 7 that for all films, the n value gradually increased with the rise of λ in the UVR and a peak behavior was observed at around 380 nm, then the n value decreased in the VR. After 650 nm wavelength, it became sturdy or nearly even in the VR and near IR region. The similar peak behavior of the refractive index for CBD-deposited PZS and CDZS thin films was reported by Jrad et al. [50] and the computed maximum n value was about 2.4. In another study [51], the maximum n value of the PZS thin films prepared through CBD method was found to be 1.35. However, the n value is comparatively lower in our sample (nearly 1.20).

The reason for decrease in n value might be attributed to the formation of non-stoichiometric oxide phases in the ZnS films [52].

3.5.4. Absorption coefficient

The absorption coefficient, α can be estimated by using the following equation (8) [53]:

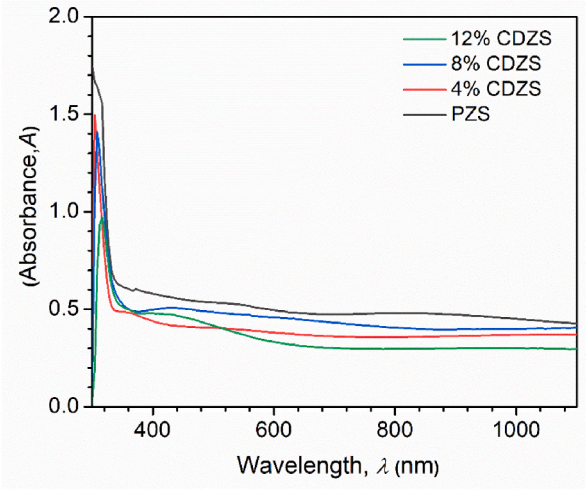

Fig. 5. Absorbance spectra (A) of PZS and CDZS thin films at different DC.

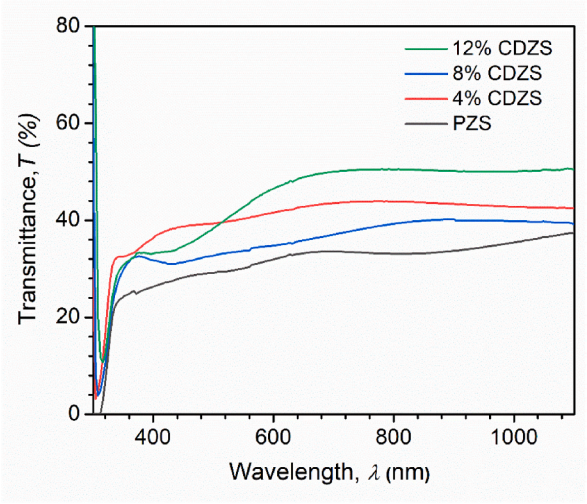

Fig. 6. Transmittance (*T*%) of PZS and CDZS thin films at diverse DC.

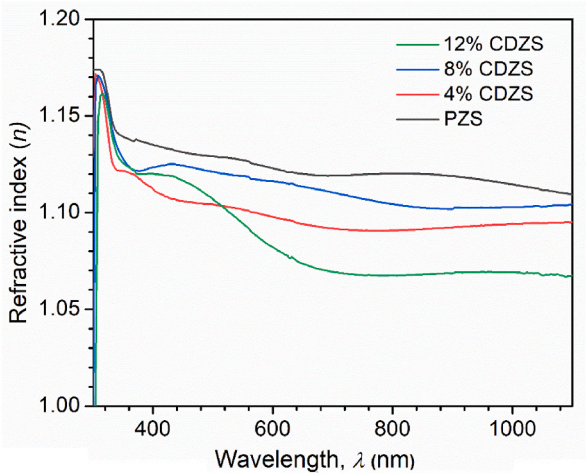

Fig. 7. Refractive index of PZS and CDZS thin films at different DC.

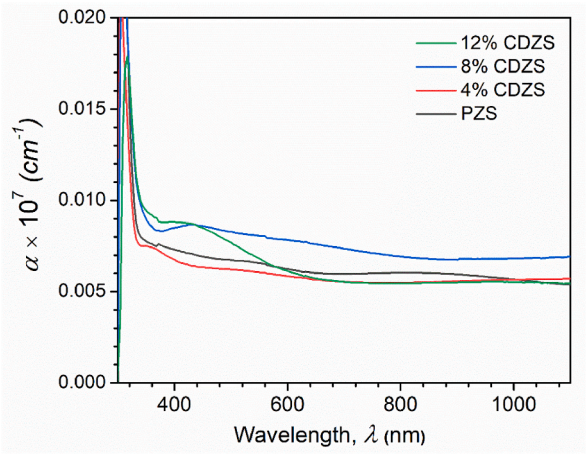

Fig. 8. Absorption coefficient of PZS and CDZS thin films at different DC.

$$\alpha = \frac{2.303A}{d} \tag{8}$$

Where, d is the thickness of the TF. The plot of α vs λ is presented in Fig. 8. In this Fig.,the value of α decreased with increasing λ and it becomes almost flat after 800 nm. The TF shows high absorption for wavelength below the VR.

3.5.5. Optical energy bandgap

The optical band gap energy, E_g of the prepared samples was determined using the Tauc relation (9) [54]:

$$\alpha h\upsilon = k\left(h\upsilon - E_g\right)^n \tag{9}$$

Where, k is a constant and the value of n is equal to ½ since the transition in the present case is direct allowed.Where, k is a constant. The value of E_g was resolved via deriving the linear part of the plots $(\alpha h\upsilon)^2$ *vs* $h\upsilon$ curve to zero α value (Fig. 9). In Fig. 9, the E_g values were found within the range of 3.63-3.38 eV respectively for PZS and CDZS thin films at diverse DC (Table 2). The value of E_g decreased with adding DC in PZS. The reduction of E_g with rising DC may be ascribed to the slight upsurge in the crystallite size as calculated from the XRD pattern and/or the amalgamation of a slight quantity of oxygen interstitially in the PZS, creating an imperfection level in the E_g. In earlier research, the E_g value of the CBD deposited PZS thin film was found to be 4.01 eV, whereas in our study it decreases, which may be due to modification of deposition condition [40].

3.5.6. Extinction coefficient

The extinction coefficient (k) can be computed by using the following equation (10) [55]:

$$k = \frac{\alpha\lambda}{4\pi} \tag{10}$$

Fig. 10 presented the variation of k with λ for PZS and CDZS thin films. It is observed that the value of k decreased deliberately at the starting of VR and after reaching a minimum value it increased with the increase of wavelength. Another observation is that k is relatively high in the IR region, a close-fitting medium transparent attribute of the prepared TF which well matches with the transmission.

3.5.7. Dielectric constant

The dielectric constant, ε of a material is connected with the density of states inside the E_g
and rely on the electronic assembly of that material and can be expressed by the following relation (11) [56]:

$$\varepsilon = \varepsilon_1 + i\varepsilon_2 \tag{11}$$

where ε_1 is real and ε_2 is imaginary part of dielectric constant and these two quantities can be found out by using the following equations (12) and (13) [57]:

$$\varepsilon_1 = n^2 - k^2 \tag{12}$$

$$\varepsilon_2 = 2nk \tag{13}$$

Fig. 11 (a, b) respectively presented the(a) real and (b) imaginary part of ε for PZS and CDZS thin films as a function of λ at different DC. In Fig, 11a, it can be noticed that with the increase of λ, the ε_1 value gradually increased up to VR after that it falls at the IR region. The maximum ε_1 value is observed for 12 % CDZS thin film at VR. Conversely, In Fig, 11b, ε_2 value firstly increased close to 380 nm and after that gradually declined with increasing λ. A sharp peak is also detected at about 380 nm in both cases. Another observation is that for all TFs the values of ε_1 are higher in comparison to ε_2.

3.6. Electrical properties

3.6.1. I–V characteristics

Fig. 12 demonstrated the current (I) -voltage (V) characteristics curve for PZS and CDZS thin films with different DC. The obtained I–V curves are linear prior to the working range of functional voltage, which implies that the samples exhibit an ohmic nature. Moreover, the resistivity (ρ) of the deposited TF is around 10^5 Ωm. These consequences are analogous to previously reported values (10^6–10^{14} Ωm) [58,59]. The greater value of ρ may be ascribed by the nano crystallinity of TF, grain edge gaps, existence of exterior states and lesser d of the film signifying the suitability of the PZS and CDZS namely buffer layer in the TF technology [60].

4. Conclusions

PZS and CDZS thin films have been fruitfully deposited on glass substrates through CBD technique by varying DC. XRD patterns revealed the hexagonal structure of deposited TF. The crystallite size and lattice parameter of the CDZS thin films decreased in comparison to PZS which might be due to the enhancement of strain in the film. The dislocation density and number of crystallites per unit area also increased due to co-doping. SEM images presented the spherical shape agglomerates and cracks for PZS thin film whereas

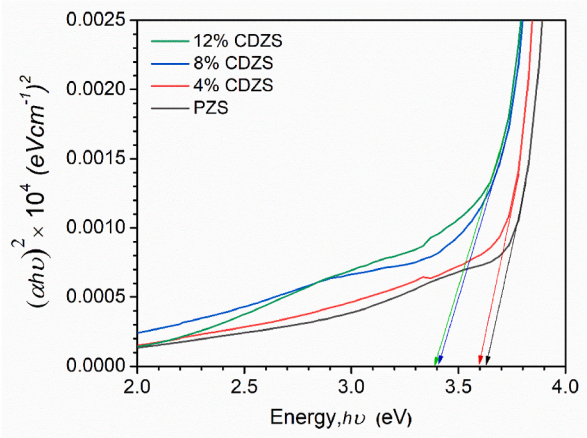

Fig. 9. $(\alpha h\upsilon)^2$ vs $h\upsilon$ plot of PZS and CDZS thin films at different DC.

Table 2
Optical direct band gap for different samples.

Types of TF samples	Direct Energy Band Gap (eV)
PZS	3.63
4 % CDZS	3.60
8 % CDZS	3.41
12 % CDZS	3.38

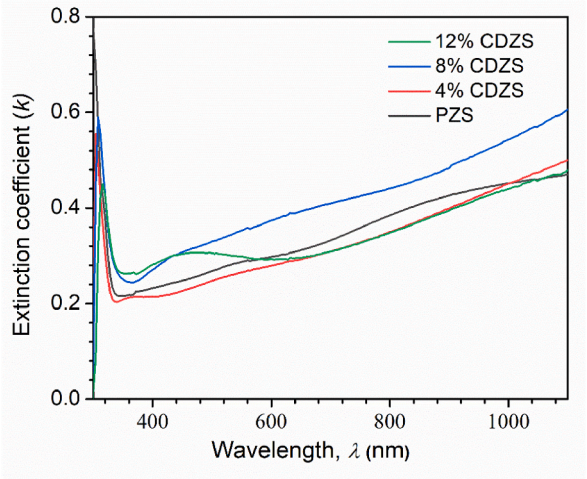

Fig. 10. Extinction coefficient vs wavelength curve of PZS and CDZS thin films at different DC.

CDZS thin films cracks were not noticed. AFM confirmed fairly distributed small-sized grains with RMS roughness of 28 nm. The existence of Zn, S and Co were identified through EDX analysis. From Uv–vis spectroscopic analysis, it is noticed that all TFs have higher *T%* values in the visible range and the maximum *T%* is about 50 % for 12 % CDZS thin film at 750 nm. The calculated E_g values were found in the range of 3.38–3.63 eV for deposited TFs. The value of E_g decreased with increasing DC in PZS. The reduction of E_g with increasing DC might be attributed to the slight increase in the *D* creating a defect level in the E_g. With the increase of λ, the ε_1 value gradually increased up to VR after that it fell at IR. Conversely, ε_2 value firstly increased close to 380 nm and after that gradually declined. The values of ε_1 are higher in comparison to ε_2. DC electrical analysis demonstrated that the TFs are semiconducting in nature partaking the resistivity (ρ) of the deposited TF is around 10^5 Ωm. Finally, it can be signified that the prepared CDZS thin films may be suitable as a window material in the manufacture of solar cells and optoelectronic devices.

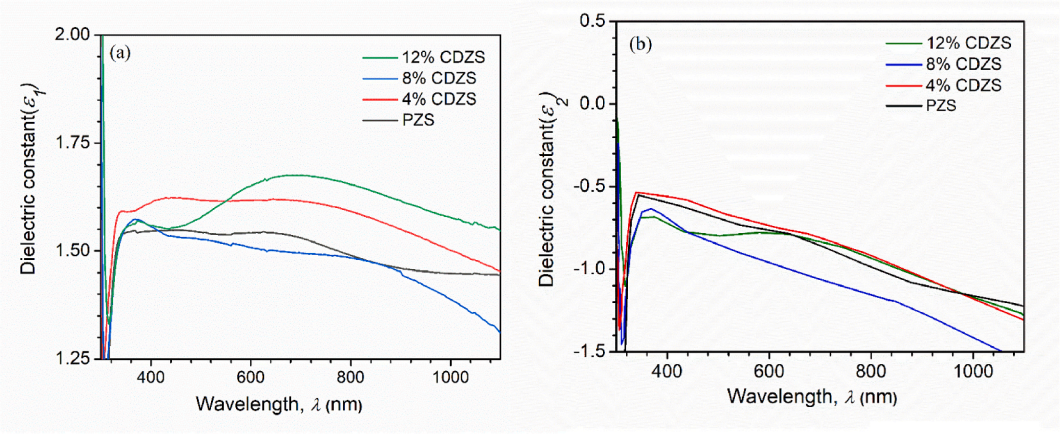

Fig. 11. Dielectric constant (a) real part and (b) imaginary part of PZS and CDZS thin films at different DC.

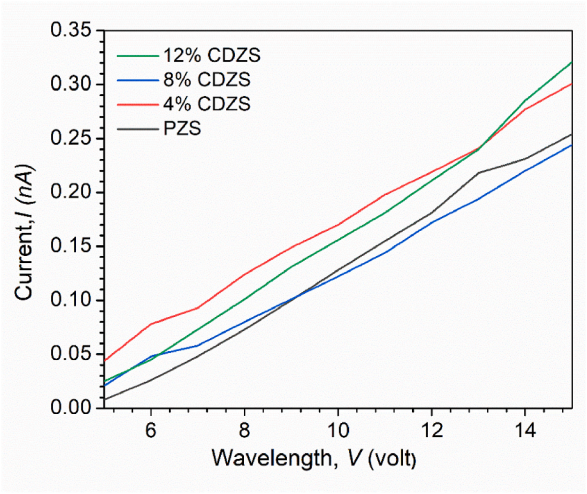

Fig. 12. I–V curves of PZS and CDZS thin films at different DC.

Compliance with ethical standards

The authors confirm that the submitted manuscript is an outcome of research work carried out in our laboratories. The results have not been published in whole or in part elsewhere. The manuscript is not currently being considered for publication in another journal. All authors have been personally and actively involved in substantive work leading to the manuscript and will hold themselves jointly and individually responsible for its content.

Data availability statement

Data will be made available on request.

CRediT authorship contribution statement

Rahima Nasrin: Writing – review & editing, Supervision, Conceptualization. **Lamiya Khan:** Writing – original draft, Methodology, Investigation, Formal analysis. **Md Obaydul Haq:** Formal analysis, Data curation. **Md Mohiuddin:** Writing – review & editing, Investigation. **Humayun Kabir:** Writing – review & editing, Conceptualization.

Declaration of competing interest

The authors declare that they have no known competing financial interests or personal relationships that could have appeared to influence the work reported in this paper.

Acknowledgments

The authors are indebted to the World Academy of Science (TWAS), Trieste, Italy, for providing the optical and electrical characterization instrument used for this study. The authors acknowledge the support of the BCSIR and professor Dr Khandker Sadat Hossain, Dept. of Physics, University of Dhaka respectively for providing the structural characterization and AFM analysis facilities respectively.

References

[1] S. Kumar, D.K. Aswal, Thin film and significance of its thickness, Recent Advances in Thin Films (2020) 1–12, https://doi.org/10.1007/978-981-15-6116-0.
[2] Z.K. Heiba, M.B. Mohamed, S.I. Ahmed, A.M. El-Naggar, A.A. Albassam, Effect of Mg and Cu doping on structural, optical, electronic and thermal properties of ZnS quantum dots, J. Mater. Sci. Mater. Electron. 31 (1–6) (2020) 14746.
[3] R. Nasrin, A.H. Bhuiyan, Evaluation of electrical carrier transport mechanism in plasma polymerized *n*-butyl methacrylate thin films, Polym. Sci. 60 (6) (2018) 882–889.
[4] T. Taguchi, Y. Yamada, T. Ohno, J.T. Mullins, Y. Masumoto, Ultraviolet laser and photodetector of CdZnS/ZnS multiple quantum wells, Physica B 191 (1993) 136–139.
[5] K. Ichino, T. Kojima, S. Obata, T. Kuroyanagi, S. Nakazawa, S. Kashiyama, ZnS based ZnSTe :N/n-ZnS light emitting diodes, APEX 6 (2013) 112–120.
[6] K. Naseemam, K. Ribin, N. Navya, P. Prasannan, Thermal coversion of CBD grown ZnS thin films to ZnO, J. Z. Naturforsch. 76 (2021) 65–73.
[7] Y. Kavanagh, M.J. Alam, D.C. Cameron, The characteristics of thin film electroluminescent displays produced using sol-gel produced tantalum pentoxide and zinc sulfide, Thin Solid Films 85 (2004) 447–448.
[8] M.M. Islam, S. Ishizuka, A. Yamada, K. Sakurai, S. Niki, T. Sakurai, K. Akimoto, CIGS solar cells with MBE grown ZnS buffer layer, Sol. Energy Mater. Sol. Cells 93 (2009) 970–972.
[9] J. Rufat, Properties in Fe-doped ZnS thin films, Res. Dev. Mater. Sci. 16 (2021). RDMS.000879.
[10] R. Sahraei, S. Darafarin, Preparation of nanocrystalline Ni doped ZnS thin films by ammonia-free chemical bath deposition method and optical properties, J. Lumin. 149 (2014) 170–175.
[11] A. Goudarzi, G.M. Aval, S.S. Park, M.C. Choi, R. Sahraei, M.H. Ullah, A. Avane, C.S. Ha, Low-temperature growth of nanocrystalline mn-doped zns thin films prepared by chemical bath deposition and optical properties, Chem. Mater. 21 (2009) 2375–2385.
[12] O.I.D. Grijalv, D.B. Mendoza, A.F. Pacheco, R.L. Delgado, A.R. Carrazco, M.E.A. Ramos, Cu-doped CdS thin films by chemical bath deposition and ion exchange, J. Mater. Sci. Mater. Electron. 31 (2020) 1722–1730.
[13] Z.K. Heiba, M.B. Mohamed, A. Badawi, Effect of preparation temperature on the structural, optical and electronic properties of CDZnS nanostructures, Chem. Phys. Lett. 775 (2021) 138653–138656.
[14] T.T. Nguyen, X.A. Trinh, L.H. Nguyen, T.H. Pham, Photoluminescence characteristics of as-synthesized and annealed zns: cu, al nanocrystals, Adv. Nat. Sci. Nanosci. Nanotechnol. 2 (2011) 035008. Article ID.
[15] M.A. Shakil, S. Das, M.A. Rahman, U.S. Akther, M.K.H. Majumdar, M.K. Rahman, Review on zinc sulphide thin film fabrication for various applications based on doping elements, Mater. Sci. Appl. 9 (2018) 751–778.
[16] V. Ramasamy, K. Praba, G. Murugadoss, Synthesis and study of optical properties of transition metals doped zns nanoparticles, Spectrochim. Acta 96 (2012) 963–971.
[17] S.V. Trukhanov, A.V. Trukhanov, V.A. Turchenko, AnV. Trukhanov, D.I. Tishkevich, E.L. Trukhanova, T.I. Zubar, D.V. Karpinsky, V.G. Kostishyn, L.V. Panina, D. A. Vinnik, S.A. Gudkova, E.A. Trofimov, P. Thakur, A. Thakur, Y. Yang, Magnetic and dipole moments in indium doped barium hexaferrites, J. Magn. Magn Mater. 457 (2018) 83–96.
[18] A. Goktas, I.H. Mutlu, Structural, optical, and magnetic properties of solution-processed co-doped ZnS thin films, J. Electron. Mater. 9 (2016) 772–778, https://doi.org/10.1007/S11664-016-4771-3.
[19] A.I. Inamdar, S. Lee, D. Kim, K.V. Gurav, Metal-doped ZnS thin films on glass substrates using chemical bath deposition, Thin Solid Films 537 (2013) 36–41.
[20] P. O'Brien, D.J. Otway, D.S. Boyle, The importance of ternary complexes in defining basic conditions for the deposition of ZnS, Thin Solid Films 361 (2000) 17–21.
[21] C.D. Lokhande, H.M. Pathan, M. Giersig, H. Tributsch, Preparation of Znx(O,S)y thin films using modified chemical bath deposition method, Appl. Surf. Sci. 187 (2002) 101–107.
[22] C. Rodriguez, M.G. Sandovalc-Paz, G. Cabello, M. Flores, H. Fernandez, C. Carrasco, Characterization of ZnS thin films synthesized through a non-toxic precursors chemical bath, Mater. Res. Bull. 60 (2014) 313–321.
[23] H. Haddad, A. Chelouche, D. Talantikite, H. Merzouk, F. Boudjouan, D. Djouadi, Effects of deposition time in chemically deposited ZnS films in acidic solution, Thin Solid Films 89 (2015) 451–456.
[24] Y. Kavanagh, D.C. Cameron, Zinc sulfide thin films produced by sulfidation of sol–gel deposited zinc oxide, Thin Solid Films 398 (2001) 24–28.
[25] Y.F. Nicolau, Solution deposition of thin solid compound films by a successive ionic-layer adsorption and reaction process, Appl. Surf. Sci. 22 (1985) 1061–1074.
[26] S. Yano, R. Schroeder, Ullrich and Sakai, Absorption and photocurrent properties of thin ZnS films formed by pulsed-laser deposition on quartz, Thin Solid Films 423 (2003) 273–276.
[27] R.S. Mane, C.D. Lochande, Chemical deposition method for metal chalcogenide thin films, Mater. Chem. Phys. 65 (2000) 1–31.
[28] K.B. Bacha, A. Timoumi, N. Bitri, H. Bouzouita, Structural, morphological and optical properties of sprayed ZnS thin films on various substrate natures, Optik 126 (2015) 3020–3024.
[29] C.T. Hsu, Epitaxial growth of II–VI compound semiconductors by atomic layer epitaxy, Thin Solid Films 335 (1998) 284–291.
[30] R.Y. Mohammed, Annealing effect on the structure and optical properties of CBD-ZnS thin films for windscreen coating, Materials 14 (2021) 6748–6755.
[31] S. Aksay, S.A. Pehlivanoglub, T. Hurma, The structural and optical properties of ZnO:Sn nanostructured films by MW-CBD, J. Mol. Struct. 1225 (2021), 129227-7.
[32] A. Ashok, G. Regmi, A. Romero-Núñez, M. Solis-López, S. Velumani, H. Castaneda, Comparative studies of CdS thin films by chemical bath deposition techniques as a buffer layer for solar cell applications, J. Mater. Sci. Mater. Electron. 31 (2020) 7499–7518.
[33] K.H. Maria, P. Sultana, M.B. Asfia, Chemical bath deposition of aluminum doped zinc sulfide thin films using non-toxic complexing agent: effect of aluminum doping on optical and electrical properties, AIP Adv. 10 (2020) 65315–65316.
[34] R. Nasrin, M.O. Haq, M. Mohiuddin, H. Akther, Effect of deposition parameter on exterior morphology, structural and optical characteristics of chemical bath deposited zinc oxide thin films, Surf. Rev. Lett. (2024) 2450059.
[35] F. Long, W. Wang, Z. Cui, L. Fan, Z. Zou, T. Jia, An improved method for chemical bath deposition of ZnS thin films, Chem. Phys. Lett. 462 (2008) 220–228.
[36] M.S. Akhtar, Y.G. Alghamdi, M.A. Malik, R.M.A. Khalil, Saira Riazb, S. Naseem, Structural, optical, magnetic and half-metallic studies of cobalt doped ZnS, J. Mater. Chem. C 3 (2015) 6755–6763.
[37] S. Mardix, Polytypism: a controlled thermodynamic phenomenon, Phys. Rev. B 33 (1986) 8677–8683.
[38] M. Wang, L. Jiang, E.J. Kim, S.H. Hahn, Electronic structure and optical properties of $Zn(OH)_2$: LDA+*U* calculations and intense yellow luminescence, RSC Adv. 5 (2015) 87496–87503.
[39] M.H. Khalil, R.Y. Mohammed, M.A. Ibrahem, The influence of CBD parameters on the energy gap of ZnS narcissus-like nanostructured thin films, Coatings 9 (2021) 1131–1139.

[40] F. Göde, E. Güneri, A. Kariper, C. Ulutaş, F. Kirmizigül, C. Gümü, Influence of annealing temperature on the structural, optical and electrical properties of amorphous Zinc Sulfide thin films, J. Phys. (Paris): Conf. Series 326 (2011) 012020.
[41] B.D. Cullity, Elements of X-Ray Diffraction, Addision-Wesley Publishing Co. Inc, 1967, p. 65.
[42] A.V. Trukhanov, V.O. Turchenko, I.A. Bobrikov, S.V. Trukhanov, I.S. Kazakevich, A.M. Balagurov, Crystal structure and magnetic properties of the $BaFe_{12-x}Al_xO_{19}$ (x=0.1–1.2) solid solutions J, Magnetism and Magnetic Mater. 393 (2015) 253–259.
[43] P. Kathirvel, D. Manoharam, S.M. Mohan, S. Kumar, Spectral investigations of chemical bath deposited zinc oxide thin films ammonia gas sensor, J. Optoelectron. Biomed. Mater. 1 (2009) 25–33.
[44] T.E. Manjulavalli, A.G. Kannan, Structural and optical properties of ZnS thin films prepared by chemical bath deposition method, Int. J. ChemTech Res. 8 (2015) 396–402.
[45] S.M. Kabbur, S.D. Waghmare, U.R. Ghodake, S.S. Suryavanshi, Synthesis, morphology and electrical properties of Co^{2+} substituted NiCuZn ferrites for MLCI applications, AIP Conf. Proc. 1942 (2018) 130002–130009.
[46] A. Mukherjee, M. Partha, Characterization of Sn doped ZnS thin films synthesized by CBD, Mater. Res. 20 (2017) 430–435.
[47] U.N. Maiti, P.K. Ghosh, S.F. Ahmed, M.K. Mitra, K.K. Chattopadhyay, Structural, optical and photoelectron spectroscopic studies of nano/micro ZnO:Cd rods synthesized via sol-gel route, J. Sol. Gel Sci. Technol. 41 (2007) 87–92.
[48] R. Nasrin, A.H. Bhuiyan, Synthesis of iodine doped n-BMA th n films via plasma polymerization technique: effect on optical properties, Surf. Rev. Lett. 27 (2020) 1950133.
[49] F. Göde, C. Gümüşa, Influences of copper and manganese concentrations on the properties of polycrystalline ZnS:Cu and ZnS:Mn thin films, J. Optoelectron. Adv. Mater. 11 (2009) 429–436.
[50] A. Jrad, M. Naouai, A. Abdullah, S. Ammar, N.T. kamoun, Doping ZnS films with cobalt: structural, compositional, morphological, optical, electrical, magnetic and photocatalytic properties, Physica B: Condenser 603 (2021) 412776.
[51] F. Göde, C. Gümüşa, M. Zor, Influence of the thickness on physical properties of chemical bath deposited hexagonal ZnS thin films, J. Optoelectron. Adv. Mater. 9 (2007) 2186–2191.
[52] O.L. Arena, M.T.S. Nair, P.K. Nair, Chemical bath deposition of ZnS thin films and modification by air annealing, Semicond. Sci. Technol. 12 (1997) 1323.
[53] R. Nasrin, A.H. Buiyan, Effect of heat treatment on infrared and ultraviolet-visible spectroscopic studies of the PPnBMA thin films, A. Phys. A 124 (2018) 856–862.
[54] H. Akther, M.M. Rahman, A.H. Bhuiyan, H. Kabir, S.M.A. Al Zumahi, J.A. Syed, R. Nasrin, Carrier transport mechanisms of iodine-doped plasma polymerised N, N, 3, 5 tetramethylaniline thin films, Mater. Today Commun. 31 (2022) 103377.
[55] H. Akther, A.H. Bhuiyan, H. Kabir, R. Nasrin, M.M. Rahman, Understanding the enhancement of the optical and electronic attributes of iodine-doped vacuum deposited tetramethylaniline (PPTMA) thin film coatings, J. Alloys Compd. 874 (2021) 159989.
[56] J.O. Emegha, E.D. Elete, F.O.O. Efe, A.C. Adebisi, Optical and electrical properties of semiconducting ZnS thin film prepared by chemical bath deposition technique, J. Mat. Sci. Res. Rev. 4 (2019) 1–8.
[57] R. Nasrin, A.H. bhuiyan, Thermal and AC electrical properties of thin films prepared from n-butyl methacrylate by a capacitively coupled plasma reactor, Surf. Rev. Lett. 26 (2019) 1850146.
[58] M. Taskin, J. Podder, Dielectric properties of pristine and cobalt doped zinc oxide thin films prepared by spray pyrolysis, Appl. Sci. Rep. 3 (2014) 112–116.
[59] S. Chaliha, M. Borah, P.C. Sarmah, Optical and electrical properties of thermally evaporated ZnSe Thin films, Indian J. Phys. 82 (2008) 303–310.
[60] O. Pc, E. Aj, E. Pa, Effect of manganese percentage doping on thickness and conductivity of zinc sulphide nanofilms prepared by electrodeposition method, Int. J. Sci. Res. 4 (2014) 2275–2279.